Wetterlind Johanna (Orcid ID: 0000-0003-2821-2999)
Viscarra Rossel Raphael A. (Orcid ID: 0000-0003-1540-4748)

Diffuse reflectance spectroscopy characterises the functional chemistry of soil organic carbon in agricultural soils

J. WETTERLIND[a], R. A. VISCARRA ROSSEL[b], MARKUS STEFFENS[c]

[a]*Department of Soil and Environment, Swedish University of Agricultural Science, PO Box 234, SE-532 23 SKARA, Sweden,*

[b]*Soil and Landscape Science, School of Molecular and Life Sciences, Curtin University, GPO Box U1987, Perth WA 6845, Australia.*

[c]*Department of Soil Sciences, Research Institute of Organic Agriculture FiBL, Ackerstrasse 113, 5070 Frick, Switzerland.*

Correspondence: Johanna Wetterlind. E-mail: johanna.wetterlind@slu.se

This article has been accepted for publication and undergone full peer review but has not been through the copyediting, typesetting, pagination and proofreading process which may lead to differences between this version and the Version of Record. Please cite this article as doi: 10.1111/ejss.13263

Summary

Soil organic carbon (SOC) originates from a complex mixture of organic materials, and to better understand its role in soil functions, one must characterise its chemical composition. However, current methods, such as solid-state ^{13}C nuclear magnetic resonance (NMR) spectroscopy, are time-consuming and expensive. Diffuse reflectance spectroscopy in the visible and infrared regions (vis–NIR: 350–2500 nm; mid-IR: 4000–400 cm^{-1}) can also be used to characterise SOC chemistry; however, it is difficult to know the frequencies where the information occurs. Thus, we correlated the C functional groups from the ^{13}C NMR to the frequencies in the vis–NIR and mid-IR spectra using two methods: 1) 2-dimensional correlations of ^{13}C NMR spectra and the diffuse reflectance spectra, and 2) modelling the NMR functional C groups with the reflectance spectra using support vector machines (validated using 5 times repeated 10-fold cross-validation). For the study, we used 99 mineral soils from the agricultural regions of Sweden. The results show clear correlations between organic functional C groups measured with NMR and specific frequencies in the vis–NIR and mid-IR spectra. While the 2D correlations showed general relationships (mainly related to the total SOC content), analysing the importance of the wavelengths in the SVM models revealed more detail. Generally, models using mid-IR spectra produced slightly better estimates than the vis–NIR. The best estimates were for the alkyl C group (R^2 = 0.83 and 0.85, vis–NIR and mid-IR, respectively), and the O/N-alkyl C group was the most difficult to estimate (R^2 = 0.34 and 0.38, vis–NIR and mid-IR, respectively). Combining ^{13}CNMR with the cost effective diffuse reflectance methods could potentially increase the number of measured samples and improve the spatial and temporal characterisation of SOC. However, more studies with a wider range of

soil types and land management systems are needed to further evaluate the conditions under which these methods could be used.

Keywords: C functional groups, 13C NMR, C turnover, mid-IR spectroscopy, NIR spectroscopy, soil organic matter quality, soil organic matter composition

Introduction

Soil organic matter consists of a wide range of heterogeneous materials in all stages of decomposition, closely interacting with the soil mineral matrix (Lehmann & Kleber, 2015). To better understand the mechanisms controlling C dynamics, we need information on the chemical composition of the soil organic carbon (SOC), the soil physicochemical properties and environmental factors (Paré & Bedard-Haughn, 2013; Viscarra Rossel *et al.*, 2019; Schmidt *et al.*, 2011; Kögel-Knabner & Rumpel, 2018). This study pertains to the characterisation of organic functional groups in SOC.

Solid-state ^{13}C Nuclear Magnetic Resonance (NMR) spectroscopy is a powerful experimental technique used in different disciplines to elucidate the atomic and molecular structure of a wide range of substances. The main advantages of NMR spectroscopy are that it is non-destructive and the sample can be used for other experiments, solid and liquid samples can be analysed; no extractions are needed and it gives comprehensive and semi-quantitative information on the chemical composition of a sample for one or several selected elements. It is commonly used to quantitatively determine the chemical composition of SOC (Bonanomi *et al.,* 2013), to deduce SOC's degree of decomposition and to allow an estimation of more resistant fractions. Weng *et al.* (2021) stressed the point that NMR was used to prove and disapprove various theories and hypothesis on SOC dynamics and stabilisation. The technique does not provide the structural organization of SOC on a molecular level

but can broadly differentiate C functional groups (Audette *et al.*, 2021). Most studies identify alkyl C, O/N-alkyl C, aromatic C and carbonyl C groups (Audette *et al.*, 2021; Baldock *et al.*, 1992; Kögel-Knabner, 1997, 2000). Chemical shift ranges can be fitted to four spectral regions, labeled as (1) alkyl C (10–45 ppm; long chain polymethylene type structures, e.g. fatty acids, waxes and resins); (2) O-alkyl C (45–110 ppm; mostly carbohydrates); (3) aromatic C (110–160 ppm; protonated and C substituted aromatics and unsaturated C and oxygenated aromatics); and (4) carboxyl C (160–200 ppm; carboxylic C, esters and amides) (Baldock *et al.*, 1992; Oades *et al.*, 1987).

Baldock *et al.* (1997) evaluate the potential of solid-state ^{13}C NMR spectroscopy to assess the extent of decomposition of natural organic matter. They describe a strong link between the progressing decomposition of natural organic matter, relative increase in alkyl C and relative decrease in O-alkyl C. This can be explained by the characteristic hydrophobicity and more resistant alkyl materials on the one side and the easily decomposable nature of polysaccharides and proteins on the other side. In a recent meta-analysis, Audette et al. (2021) draw a comprehensive summary of the origin and lability of the NMR derived functional C groups and showed a clear influence on the proportions of the different ^{13}C NMR derived C groups of changes in agricultural management practises (i.e. fertilisation, tillage, crop rotation and liming), demonstrating the usefulness of this type of information for guiding agricultural practises and improving soil health.

Due to the small content of total SOC in soil samples and the low natural abundance of the ^{13}C isotopes, the measurement with an NMR can be slow, which limits the number of samples that can be analysed, restricting the use of the method to smaller dedicated studies (Baldock *et al.*, 1989; Kinchesh *et al.*, 1995). In addition,

paramagnetic materials such as iron may interfere with the measurements further reducing the signal-to-noise ratio, so that they have to be removed by treating the samples with hydrofluoric acid (HF) (Mathes *et al.*, 2002). This treatment results in an increase in SOC content; however, it is also associated with varying degrees of SOC loss, both in terms of total loss and selective loss of organic compounds. This may result in biased interpretation of the SOC chemical composition (Sanderman *et al.*, 2017).

Diffuse reflectance spectroscopy in the visible, near and mid-infrared (vis–NIR: 350–2500 nm or 28571–4000 cm^{-1}; mid-IR: 2500–25000 nm or 4000–400 cm^{-1}) are rapid, non-destructive, methods commonly used in soil science (Soriano-Disla *et al.*, 2014). Reflectance spectra in the mid-IR region are the result of interactions between the radiating energy and the bonds in molecules of soil constituents. In the NIR, the spectra result from overtones and combinations of the fundamental vibrations in the mid-IR region, while in the visible range the primary processes are electronic excitations (Stenberg *et al.*, 2010). The methods provide qualitative information on the fundamental composition of the soil, including clay and iron oxide minerals, organic matter, water and particle size. Hence, that information is the basis for creation of models from the spectra used to estimate several properties. However, the information in the diffuse reflectance spectra is overlapping and complex, and calibration models are needed for quantitative analysis. Absorbance is bond specific, but is also affected by the type of functional group, its neighbouring molecules and hydrogen bonds (Miller, 2001). Information on SOC can be found in several regions of the mid-IR and vis–NIR spectra, and corresponds to, for example, –CH and –CO groups. SOC content is one of the most commonly modelled and best predicted soil properties using these techniques (Stenberg *et al.*, 2010). Because the information is

related to specific molecular bonds and their surrounding chemistry, SOC content is in fact predicted by its chemical composition, and a number of studies have shown the potential for vis–IR spectroscopy to predict different aspects of the organic matter quality (Knox *et al.*, 2015; Viscarra Rossel & Hicks, 2015). The possible advantage of reflectance spectroscopy for characterising the composition of soil organic C is that the chemical information in a soil sample might be gained from the analysis of the whole soil without C fractionation (e.g. into particulate, mineral associated or pyrogenic organic C), or HF-treatment.

We found a number of studies that explored the relationship between vis–NIR or mid-IR spectra and solid state ^{13}C NMR spectra (Leifeld, 2006; Terhoeven-Urselmans *et al.*, 2006; Forouzangohar *et al.*, 2013, 2015; Kang *et al.*, 2017; Ludwig *et al.*, 2008). These studies used HF-treated mineral soils (for both solid state ^{13}C NMR and the vis-NIR and mid-IR spectroscopy) or specific soil C fractions, e.g. litter, particulate and mineral-associated organic carbon. To our knowledge, there are no other published studies on the characterisation of soil organic C chemistry with spectroscopy focusing on whole agricultural soils.

Given this research gap, our aim here was to test if vis–NIR and mid-IR diffuse reflectance spectroscopy could characterise the functional chemistry of SOC in whole arable soils with as little pre-treatment as possible, i.e. without HF-treatments or soil C fractionation. To do so, we derived 2-dimensional correlations of solid state ^{13}C NMR spectra and vis–NIR and mid-IR spectra, compared assignments of the NMR functional organic C groups and the corresponding frequencies in the vis–NIR and mid-IR, and modelled the NMR functional groups with the reflectance spectra using support vector machine regression. For our experiments, we used 99 Swedish soil samples with a wide range in SOC content.

Materials and methods

Soil samples and analyses

We used 99 mineral soil samples from the 0-20 cm layer of agricultural fields in Sweden (Fig. 1). The soils were selected from 12,500 soil samples collected in a national campaign run by the Swedish Board of Agriculture during 2010 and 2011 and archived at the Swedish University of Agricultural Sciences. The 12,500 samples were collected in a regular grid of one soil sample per km^2, randomly moving the sampling site 1-150 m around the grid node, across about 90 % of Swedish agricultural land. The 12,500 samples were air dried, sieved to 2 mm and analysed for soil texture, soil organic matter content (measured as loss on ignition and corrected for structural water in clay (Ekström,1927)) prior to archiving. Soil texture was divided into clay (< 0.002 mm), silt (0.002–0.06 mm) and sand (0.06–2 mm). Clay content was analysed using a sedimentation method modified from Gee & Bauder (1986); the sand fraction was determined by sieving and the silt fraction was determined by difference. The 99 samples used in this study were selected using stratified random sampling to cover a wide range of soil texture and soil organic matter content by dividing the 12,500 soil samples into classes based on soil texture and organic matter content and randomly select samples within those classes (Fig. 1 and supplementary Table 1 and supplementary Figure 1). A maximum amount of organic matter was set to 16 % to focus on mineral soils and the clay content was limited to 40 % because of a focus on more sandy soils in a joint study. The 99 samples selected for this study represent a cross section of the possible variations in soil texture and organic matter content of the 12,500 Swedish arable soils (within the set organic matter content and texture boundaries). For comparison with the analyses of the functional C groups the 99 samples were also analysed for SOC. There were no

carbonates present in the soil samples and the 99 samples were analysed for SOC through dry combustion on an EuroEA elemental analyser (Hekatech GmbH, Wegberg, Germany). Swedish soil are young (i.e. mainly formed during the quartanery period) and strongly affected by processes during and after the last glacial period (Karlsson *et al.*, 2021).

vis–NIR and mid-IR spectroscopy

Vis–NIR Spectra (350–2500 nm; 28571 to 4000 cm^{-1}) were determined using an ASD FieldSpec Pro FR scanning instrument (Malvern Panalytical Ltd, Malvern, UK) on the 2 mm sieved and air-dried soil samples. The instrument was equipped with a bare optic fibre connected to a probe with a 20 W Al-coated halogen tungsten light source placed 7 cm over the sample, resulting in a field of view of approximately 7.5 cm^2. Reflectance spectra were recorded in relation to an external white reference (Spectralon®) and each composite sample spectrum was comprised of 100 averaged spectra collected from a rotating sample. The spectra were sampled at 1.4–2 nm intervals with a spectral resolution of 3–10 nm. A wavelength interval of 1 nm was interpolated to the instrument output file, resulting in spectra consisting of one data point every nanometre. The vis–NIR spectra were transformed to apparent absorbance through log(reflectance^{-1}) and the 350–400 nm wavelength range was removed from further analysis due to noise.

Mid-IR spectra were recorded on four ground (< 0.5 mm) replicates of each sample using a FT-IR Vertex70 spectrometer (Bruker, Germany) with a spectral range of 1333–16667 nm (7500–600 cm^{-1}) and a spectral resolution of 4 cm^{-1} and 64 measurements per minute. The spectrometer was equipped with a nitrogen gas purging system to reduce the amount of atmospheric interference in the system which reduces masking of weak spectral features by water vapour or carbon dioxide

absorption. A gold standard was used as reference. The mid-IR spectra were transformed to apparent absorbance through log(reflectance^{-1}) and only the 4000–600 cm^{-1} (2500–16700 nm) range was used in the further analysis. The four replicates were averaged to one spectrum per sample.

13C NMR spectroscopy

The sieved samples were ground < 0.630 mm using mortar and pestle prior to solid state ^{13}C NMR experiments (Bruker DSX 200 NMR spectrometer, Karlsruhe, Germany). No paramagnetic material was present in the soils and consequently no HF-treatment was required. The cross-polarisation magic angle spinning (CPMAS) technique was applied with a ^{13}C-resonance frequency of 50.32 MHz and a spinning speed of 5 kHz. A ramped ^{1}H-pulse was used during a contact time of 1 ms in order to circumvent spin modulation during the Hartmann-Hahn contact. A pulse delay of 1 s was used for all experiments and pre-experiments confirmed that the pulse delays were long enough to avoid saturation. Depending on the C contents of the samples, between 8,000 and 400,000 scans were accumulated and a line broadening of 50 Hz was applied. The ^{13}C chemical shifts were calibrated relative to tetramethylsilane (0 ppm).

Relative contributions of the various functional C groups were determined by integration of the signal intensity in their respective chemical shift regions according to Knicker *et al.* (2005). The region from 220 to 160 ppm was assigned to carbonyl (aldehyde and ketone) and carboxyl/amide C. Olefinic and aromatic C were detected between 160 and 110 ppm. O-alkyl and N-alkyl-C signals were found from 110 to 60 ppm and from 60 to 45 ppm. Resonances of alkyl C were assigned to the region 45 to 10 ppm. (Fig. 2).

As indicator for the degree of decomposition of the SOC, the alkyl C:O/N-alkyl C ratio (45 to -10 ppm)/(110 to 45 ppm) was calculated from the NMR spectra (Baldock *et al.*, 2004).

Correlations between the SOC, relative contribution of the different C groups derived from the ^{13}C NMR spectra and the Alkyl C:O/N-alkyl C ratio derived from relative contribution were calculated using Spearman correlations.

2-D correlations

The raw NMR spectra were cut to only include the chemical shifts between 0 and 220 ppm where most of the information is found. The resolution of the three types of spectra were reduced to every 7.5th nm for the apparent absorbance vis–NIR spectra, every 10th cm^{-1} for the apparent absorbance mid-IR spectra, and every 0.8th ppm for the raw NMR spectra, resulting in about 300 observations for all three spectral types. This was done to reduce the number of variables in the correlation analysis and to have a similar number of variables in all three spectra. The NMR spectra were further smoothed by a spline function and baselined using a 2nd order polynomial. The raw NMR spectra were then recalculated as relative intensity (relative to the most intense peak). Due to the shape of the mid-IR spectra these were first split into 4 regions (600–2100, 2100–2700, 2700–3720, 3720-4000 cm^{-1}) and then a baseline was applied using 1st, 2nd, 3rd, or 4th order polynomials to the different sections. After baselining the four sections were again recombined into one spectrum. To baseline the vis–NIR spectra we applied a continuum removal (Clark & Roush, 1984). The baselining was done to further highlight and define the spectral features in the different spectra. A number of different baselining and smoothing techniques were tested, and the methods providing the visually best baselined spectra without artefacts were selected. The prepossessing of the spectra were performed in the statistical software

environment R (R Core Team, 2020) and the hyperSpec (Beleites 209 and Sergo, 2020) packages. The vis–NIR and mid-IR spectra were correlated to the NMR spectra by heterospectral correlation using the 2Dshige software (2Dshige© Shigeaki Morita, Kwansei-Gakuin University, 2004-2005). The correlations were plotted in 2-D plots for interpretation.

Modelling functional C groups

The original apparent absorbance vis–NIR and mid-IR spectra were transformed and smoothed using first order Savitzky-Golay derivative with 11 smoothing points (Savitzky & Golay, 1964). First order derivative is a well-established pre-processing method in diffuses reflectance spectroscopy studies (Stenberg *et al.,* 2010). A range of smoothing points were tested on a subset of SOC variables and the number producing the best cross-validated results was used in the final modelling. The vis–NIR and the mid-IR spectra were calibrated to the different NMR derived functional C groups using support vector machines (SVM) with a radial basis function kernel (Karatzoglou *et al.*, 2006). Kernel-based learning methods use an implicit mapping of the input data into a higher dimensional feature space defined by a kernel function. With this, it is possible to derive a linear hyperplane as a decision function for non-linear problems (Vapnik, 1995). Here, we used a Gaussian radial basis function (RBF) implemented in the kernlab library of the software R. Upper and lower bounds for the optimisation of the hyperparameters, penalty (C) and sigma of the RBF were set to 0 and 10, and 0 and 1 for C and sigma, respectively. The upper and lower bounds of the C and sigma parameters were used in the caret train function in the R library caret (Kuhn, 2008) and were optimized using the Differential Evolution optimisation (Price *et al.*, 2006), implemented in the R library DEoptim (Mullen *et al.*, 2011).

The models were validated using 10-fold (random) cross validation repeated five times using the implementation in the caret library. The aggregation of the repeated cross validations generate results that are more stable and robustness. Thus we report the validation statistics and variable importance on the average of the five repeats. The validations were evaluated using the adjusted coefficient of determination (R^2) of the linear relation between the predicted and measured values, the concordance correlation coefficient (CCC), mean error (ME), the root-mean-square error (RMSE), which is a measure of the inaccuracy of the estimates and encompasses both bias and imprecision (Viscarra Rossel & McBratney, 1998). The concordance correlation coefficient combines measures of both precision and accuracy (bias) and is calculated as

$$\frac{2r\sigma_o\sigma_p}{\sigma_o^2 + \sigma_p^2 + (\mu_o - \mu_p)^2}$$

where r is the correlation coefficient between observed o and predicted p, μ_o and μ_p are the means, and σ_o^2 and σ_p^2 are the corresponding variances.

To interpret the models, we calculated their variable importance using the varImp function in the caret library (Kuhn, 2008) of R.

Results

Chemical composition of SOC

The 99 soil samples used in this study were selected from a total of little over 12,500 Swedish arable topsoils to cover a large variation in SOC content and soil texture (Fig. 1).

SOC varied from 1.3 % to 10 % and clay and sand content ranged from 5 % to 40 % and 80 %, respectively. Because soil texture, and particularly clay content, has a significant influence on the vis–NIR and mid-IR spectra, we chose to use a data set

without correlations between clay content and SOC and thus ensure independence in our analysis of SOC and it's chemical composition.

[Figure 1]

Although all samples were collected from arable fields primarily under cereal crops, the SOC composition of the soil samples was variable, as shown by the different functional carbon groups defined with ^{13}C NMR (Fig. 2 and Supplementary Table 2).

[Figure 2]

On average, the O/N-alkyl C group showed the largest contribution to the NMR spectrum. However, the alkyl C group with an average contribution of around 25 % of the SOC showed the largest variation, contributing to up to 58 % of the carbon in one sample. The NMR spectra of the soils could be classified into roughly three types depending on the contribution of the alkyl C and O/N-alkyl C groups: soil with a fairly even contribution from the two groups and soil with a primary contribution from either the alkyl C group or the O/N-alkyl C group (Fig. 2b). The carboxyl-C group constituted the smallest portion of the total SOC. The degree of decomposition indicated by the ratio between the alkyl C and the O/N-alkyl C (Baldock *et al.*, 2004) varied between 0.34 and 2.5 (supplementary Table 2).

The proportion of the alkyl C group increased with increasing SOC content (ρ=0.76, $p < 0.05$) while the remaining carbon functional groups decreased (supplementary Table 3). The exception was the large O/N-alkyl C group that was not correlated with the total SOC content (ρ =-0.15, p=0.148) and where the largest subgroup, the carbohydrates (O/N-alkyl C subgroup 2), was positively although fairly weakly, correlated to SOC (ρ =0.45, $p < 0.05$). However, the acetal-ketal C portion of the O/N-alkyl C group (O/N-alkyl C subgroup 3) was negatively correlated to SOC,

as were the other non-alkyl C groups. The strongest correlations occurred between the alkyl C group and the other functional groups. As the alkyl C group increased, the other functional groups made up a smaller portions of the SOC. However, as for the correlations with SOC content, the largest O/N-alkyl C group, (O/N-alkyl C subgroup 2), was only weakly correlated with the alkyl C group ($\rho = 0.22$, $p < 0.05$). The ratio of alkyl C to O/N-alkyl C was strongly correlated to the alkyl C group and less so with the O/N-alkyl group ($\rho = 0.98$, $p < 0.05$, and $\rho = -0.66$, $p < 0.05$, for alkyl C and O/N-alkyl C groups, respectively)

2D correlations of 13C NMR to diffuse reflectance spectra and modelling

The relationship between the infrared spectra in the vis–NIR and mid-IR regions and the NMR spectra are shown in the 2D correlation plots, Fig. 3.

[Figure 3]

The figure reveals general correlations between the functional C groups in the NMR spectra and different frequencies in the diffuse reflectance spectra. The vis–NIR spectra show the strongest positive correlations with the alkyl C group in the visible part of the spectrum with some weaker positive correlations around 2000 nm and 2300 nm (Fig. 3a). The correlations to the remaining functional C groups show an opposite pattern to the correlations with the alkyl C group. The exception is a weak positive correlation with the O/N alkyl C subgroup 2 at around 2200 nm.

The correlations between the NMR spectra and the mid-IR spectra were more detailed and less concentrated in one region of the spectrum. Although, similar to the correlations between NMR and the vis–NIR spectra, the general pattern show opposite correlations between the mid-IR spectra and the alkyl C group compared with the correlations between the mid-IR spectra and the other functional C groups

(Fig.3 b). Strong positive correlations with the alkyl C group occur in the 2800–3000 cm^{-1} and the 1300–1700 cm^{-1} regions (Fig. 3b).

The diffuse reflectance spectra in the vis–NIR and the mid-IR regions were then used, individually, to model the different NMR derived C functional C groups using SVM (Tables 1 and 2).

The best models with both the vis–NIR and mid-IR spectral regions was the alkyl C group, as a whole and especially the largest subgroup with CH_2-C (alkyl C subgroup 2) with adjusted R^2 of 0.84 and 0.92 for vis–NIR and mid-IR models, respectively (Tables 1 and 2; Fig. 4).

[Figure 4]

The importance of different wavelengths in the machine learning models (Fig. 5) also show clear contributions from the spectral regions corresponding to the asymmetric and symmetric CH-vibrations at 2930 cm^{-1} and 2850 cm^{-1}, respectively, in the mid-IR region, and their combination bands in the NIR around 2300 nm Viscarra Rossel & Behrens, 2010). This corresponds to results shown in the 2D-correlation, although in the 2D-correlation plot of the NMR to mid-IR spectra, the alkyl-C group also showed a positive correlations with the broader absorptions at 1700–1300 cm^{-1} (Fig. 3a) and the highest correlation between the vis–NIR and the alkyl-C group was actually in the visible region (Fig. 3b).

[Figure 5]

The aryl C group was the second best predicted functional C group with both vis–NIR and mid-IR models. Absorption near 1500 and 1700–1800 cm^{-1} was important for prediction. Absorptions at 1500 cm^{-1} can be attributed to aromatic C=C stretching vibrations and those near 1700 cm^{-1} to C=O stretching vibrations (Tinti *et al.*, 2015). The 2D-correlation between the NMR and mid-IR also showed weak positive

correlations between the aryl C group and the broad absorptions between 1700 and 1300 cm^{-1}.

In the carboxyl C group, predictions of the well-defined subgroup 1 produced R^2=0.63–0.64 using both vis–NIR and mid-IR spectra. However, predictions of the carboxyl C subgroup 2 were poor (R^2= 0.35–0.45), using mid-IR and vis–NIR spectra respectively. There are regions in the mid-IR spectra (e.g. 1642–1569 cm^{-1}) that are attributed to carboxylates, amongst other organic components (Tinti *et al.*, 2015). However, this was not shown in our models. Rather, the similar pattern to the alkyl-C suggest that the carboxyl C subgroups were modelled based on negative correlations with the alkyl-C group (supplementary Table 2), whereas the large carboxyl C group show more similarities with the Aryl C subgroups.

The most difficult C group to predict in these soils was the large O/N-alkyl C group including carbohydrate C and C in amino groups. However, predictions of the small O/N-alkyl C subgroup 3, representing acetal and ketal C, produced an R^2 of around 0.7 using both vis–NIR and mid-IR spectra. One of the explanations for the difficulties in predicting this large C group might be the small variation in this group in our dataset, compared to, for example, the alkyl C group.

The modelling of the alkyl C:O/N-alkyl C ratio with both vis–NIR and mid-IR spectra produced R^2 values of 0.81 –0.84, which were similar to the R^2 of the alkyl C group (Tables 1 and 2; Fig. 4c and f). This was unsurprising because of the good predictability of the alkyl C and the very large variation in this C group compared with the O/N-alkyl C group.

The wavelength regions around 2000 nm showing weak positive correlations to the alkyl C groups and around 2200 nm showing weak positive correlations with the O/N alkyl C subgroup 2 in the 2D correlation plot have been reported to be important

for OC modeling using vis–NIR (Stenberg *et al.*, 2010), however, did not show as important in any of the models in this study. Absorbance at 2033 nm can be attributed to C=O vibrations (Viscarra Rossel & Behrens, 2010). Absorbance around 2200 nm is largely effected by minerlas, e.g. illite, that is a dominating mineral in the soils in this study (Stenberg *et al.*, 2010).

Overall, models of the NMR-derived C functional groups using mid-IR were slightly better than those using vis–NIR spectra. However, the differences were not always large. The largest difference in performance of the mid-IR and vis–NIR models was for total SOC content (Tables 1 and 2; Fig.4). The mid-IR model produced estimates of SOC that were as precise as the estimates for alkyl C (R^2 = 0.86 for SOC compared with 0.85 for alkyl C). However, the estimates of SOC from the vis–NIR model were less precise (R^2 = 0.62) than the estimates of alkyl C and aryl C (Table 1 and Fig 4a and d).

Discussion

The results provide further evidence that diffuse reflectance spectroscopy in the visible and infrared can be used to estimate the chemical composition of SOC derived from ^{13}C NMR in mineral bulk soil samples. The results presented in this study are based on young soils formed from quaternary deposits without paramagnetc material and with similar land management (arable fields), although presenting a large variation in climatic conditions, SOC content and soil texture. More studies, including other soil types and land management strategies, are needed to further evaluate under what conditions the methods could be used. Our results also demonstrate that spectroscopic estimates of SOC are soundly based on its chemical composition.

Our analyses used two approaches for relating the functional C groups to the vis–NIR and mid-IR spectra. First, using 2D heterospectral correlations between ^{13}C NMR

and infrared spectra, and second, using spectroscopic models of the specific functional C groups, which were derived from the ^{13}C NMR. There was good correspondence in the results from the two methods, which strengthens our confidence in the findings.

The 2D-correlations showed the general associations between the ^{13}C NMR and vis–NIR, mid-IR spectra spectra. The interpretation of the variable importance of the spectroscopic (vis–NIR and mid-IR) models of the functional C groups were similar but they revealed more detail. For the different C-groups, many of the important wavelength regions in the models were similar (Fig. 5), but there were some notable differences, e.g. comparing the mid-IR models of aryl C and alkyl C (Fig 5b). This also suggests that the chemical composition of SOC can be characterised separately, and is not based on SOC content. However, some of the C-groups seem to be modelled largely based on indirect correlations with other C groups which have a negative effect on model robustness.

Generally, models using mid-IR spectra produced better estimates compared to vis–NIR models. This is because the fundamental vibrations occur in the mid-IR region whereas the NIR spectra result from overtones and combinations of these vibrations (Soriano-Disla *et al.*, 2014). However, the differences were often small. One reason for this could be the contribution of the visible range to the vis–NIR models. The visible region shows the strongest correlations with the NMR-spectra in the 2D-correlation plot (Fig. 3a) and the visible and short-wave NIR regions (< 1000 nm) are indicated as important regions in the models (Fig. 5a). The response in the visible region due to organic matter is broad but clear, and several studies have reported the improved modelling of SOC when the visible and the NIR regions are combined (Stenberg *et al.*, 2010). The advantage of using mid-IR compared to vis–NIR seem to be in the estimation of total SOC in datasets with a large variation in the

composition of SOC. The estimates of SOC using vis–NIR spectra appear to be better at smaller SOC concentrations, but deteriorate at SOC contents above 4 % (Fig. 4d). Ben-Dor & Banin (1995) found similar problems with using NIR spectroscopy to estimate soil organic matter in a data set with variable degree of decomposition of the organic matter depending on organic matter content. We found a clear correlation between SOC and C composition in the soils used in our study, with an increase in the proportion of alkyl C with increasing SOC content, but also an increased variation in the proportion of the alkyl C with an increase in SOC (data not shown).

The soil samples used in this study are mineral agricultural soils. The diversity of the C inputs is narrow and, as might be expected, so is the variability of the SOC. Nonetheless, the samples originate from a large geographic extent, covering different climatic regions and with diverse soil texture (Fig. 1), which introduces variability in decomposition conditions of the soils used. Apart from the O/N-alkyl C group that constituted a smaller portion of the total SOC and was less variable in our study, the proportions and ranges of the functional C groups were similar to those of studies with more diverse samples, including forest litter, specific soil fractions and soils from different land uses (Leifeld, 2006; Terhoeven-Urselmans *et al.*, 2006).

The promising but somewhat inconsistent results in the few studies published on this subject (e.g. Leifeld, 2006; Terhoeven-Urselmans *et al.*, 2006; 431 Ludwig *et al.*, 2008; Forouzangohar *et al.*, 2015; Kang *et al.*, 2017) may be attributed to the large variability within the samples, both between and within studies, and the often small number of samples used in those studies. Other studies Terhoeven-Urselmans *et al.*, 2006; Ludwig *et al.*, 2008) reported better estimates of O/N alkyl C than our study. This might be due to the relatively small variation in O/N alkyl C in our study (23–50 %) compared to those studies which included samples with more less-decomposed

material leading to higher and more variable O/N alkyl C content (33-82 %). Differences in C inputs, with more diverse materials e.g. including coniferous materials in many of the published studies, might also partly explain the differences in the accuracy of the aryl C and carboxyl C group estimates. The relatively more homogeneous C inputs and SOC of the sample set in our study might have contributed to the better estimates of the alkyl C:O/N-alkyl C ratio.

The use of HF treated soils in some of the other studies (Forouzangohar *et al.*, 2013, 2015) prevents direct comparisons to our results. However, our results are encouraging because we obtained good estimates of the alkyl C and alkyl C:O/N-alkyl C ratio in whole mineral soils without any fractionation or chemical pre-treatments (R^2 for Alkyl C = 0.83 and 0.85, and R^2 for alkyl C:O/N-alkyl C ratio = 0.81 and 0.84, for vis–NIR and mid-IR respectively). No paramagnetic material was present in the soils in this study and the results are valid for soils under similar conditions.

Conclusions

The study shows that diffuse reflectance spectroscopy in the visible and infrared can be used to estimate the chemical composition of SOC in whole mineral soil samples without C fractionation or HF-treatment. The results further demonstrate that spectroscopic estimates of SOC are soundly based on its chemical composition.

Although diffuse reflectance spectroscopy may not estimate SOC composition as accurately as ^{13}C NMR, and there is still a need for traditional methods for calibrations, the opportunity to analyse more samples due to the more cost efficient analysis could improve the detection and monitoring of changes that might otherwise be lost due to spatial variation. Diffuse reflectance spectroscopy also enables in-field measurements, which make it possible to consider in-situ measurements of SOC composition from soil that is under field condition and undergoing decomposition.

Acknowledgements

This project was funded by the Swedish Research Council Formas [Dnr. 229-2010-951 and Dnr. 2017-00887] RAVR's contribution was supported by the Australian Government through the Australian Research Council's Discovery Projects funding scheme [project DP210100420].

References

Audette, Y., Congreves, K., Schneider, K., Zaro, G. C., Nunes, A. L. P., Zhang, H. & Voroney, R. P. 2021. The effect of agroecosystem management on the distribution of c functional groups in soil organic matter: A review. *Biology and Fertility of Soils*, **57**, 881–894.

Baldock, J., Masiello, C., Gelinas, Y. & Hedges, J. 2004. Evaluation of spectral pretreatments, spectral range, and regression methods for quantitative spectroscopic analysis of soil organic carbon composition. *Spectroscopy Letters* **92** (1–4), 39–64.

Baldock, J., Oades, J., Nelson, P., Skene, T., Golchin, A. & Clarke, P. 1997. Assessing the extent of decomposition of natural organic materials using solid-state 13 c nmr spectroscopy. *Australian Journal of Soil Research,* **35**, 1061–83.

Baldock, J. A., Oades, J. M., Vassallo, A. M. & Wilson, M. A. 1989. Incorporation of Uniformly Labelled 13C-Glucose Carbon into the Organic Fraction of a Soil. Carbon Balance and CP/MAS 13C NMR Measurements. *Australian Journal of Soil Research,* **27**, 725–46.

Baldock, J. A., Oades, J. M., Waters, A. G., Peng, X., Vassallo, A. M. & Wilson, M. A. 1992. Aspects of the chemical structure of soil organic materials as revealed by solid-state 13c nmr spectroscopy. *Biogeochemistry* **16** (1), 1–42.

Beleites, C. & Sergo, V. 2020. hyperSpec: a package to handle hyperspectral data sets in *R*. R package version 0.99-20201127. URL https://github.com/cbeleites/hyperSpec

Ben-Dor, E. & Banin, A. 1995. Near-Infrared Analysis as a Rapid Method to Simultaneously Evaluate Several Soil Properties. *Soil Science Society of America Journal*, **59** (2), 364–372.

Bonanomi, G., Incerti, G., Giannino, F., Mingo, A., Lanzotti, V. & Mazzoleni, S. 2013. Litter quality assessed by solid state C-13 NMR spectroscopy predicts decay rate better than CN and LigninN ratios. *Soil Biology & Biochemistry*, **56**, 40–48.

Clark, R. & Roush, T. 1984. Reflectance spectroscopy: Quantitative analysis techniques for remote sensing applications. *Journal of Geophysical Research*, **89**, 6329–6340.

Ekström, G. 1927. Klassifikation av Svenska Åkerjordar (Classification of Swedish arable soils). Tech. Rep. 345 (Årsbok 20), *Sveriges Geologiska Undersökning*.

Forouzangohar, M., Baldock, J., Smernik, R., Hawke, B. & Bennett, L. 2015. Mid-infrared spectra predict nuclear magnetic resonance spectra of soil carbon. *Geoderma*, **247**, 65–72.

Forouzangohar, M., Cozzolino, D., Smernik, R., Baldock, J., Forrester, S., Chittleborough, D. & Kookana, R. 2013. Using the power of C-13 NMR to interpret infrared spectra of soil organic matter: A two-dimensional correlation spectroscopy approach. *Vibrational Spectroscopy,* **66**, 76–82.

Gee, G. W. & Bauder, J. W. 1986. Particle-size analysis. In: Klute, A. (Ed.), *Physical and mineralogical methods*, 2nd Edition. Soil Science Society of America, pp. 383–411.

Kang, H., Gao, H. & Yu, W. 2017. Evaluation of spectral pretreatments, spectral range, and regression methods for quantitative spectroscopic analysis of soil organic carbon composition. *Spectroscopy Letters*, **50** (3), 143–149.

Karatzoglou, A., Meyer, D. & Hornik, K. 2006. Support vector machines in r. *Journal of Statistical Software*, Articles 15 (9), 1–28.

Karlsson, C., Sohlenius, G. & Peterson Becher, G. 2021. Handledning för jordartsgeologiska kartor och databaser över Sverige, SGU-rapport 2021:17, *Sveriges Geologiska Undersökning* (SGU), Uppsala.

Kinchesh, P., Powlson, D. S. & Randall, E. W. 1995. C NMR studies of organic matter in whole soils: 13 I. Quanitation possibilities. *European Journal of Soil Science*, **46,** 125–138.

Knicker, H., Gonzalez-Vila, F., Polvillo, O., Gonzalez, J. & Almendros, G. 2005. Fire-induced transformation of c- and n-forms in different organic soil fractions from a dystric cambisol under a mediterranean pine forest (pinus pinaster). *Soil Biology & Biochemistry*, **37,** 701–718.

Knox, N. M., Grunwald, S., McDowell, M. L., Bruland, G. L., Myers, D. B. & Harris, W. G. 2015. Modelling soil carbon fractions with visible near-infrared (VNIR) and mid-infrared (MIR) spectroscopy. *Geoderma*, **239,** 229–239.

Kögel-Knabner, I. 1997. Analytical approaches for characterizing soil organic matter. *Geoderma,* **80** (3–4), 243–270.

Kögel-Knabner, I. 2000. Analytical approaches for characterizing soil organic matter. *Organic Geochemistry*, **31**, 609–625.

Kögel-Knabner, I. & Rumpel, C. 2018. Chapter one - advances in molecular approaches for understanding soil organic matter composition, origin, and

turnover: A historical overview. In: Sparks, D. L. (Ed.), *Advances in Agronomy*. Vol. **149**. Academic Press, pp. 1–48.

Kuhn, M. 2008. Building predictive models in r using the caret package. *Journal of Statistical Software*, Articles 28 (5), 1–26.

Lehmann, J. & Kleber, M. 2015. The contentious nature of soil organic matter. *Nature*, **528** (7580), 60–68.

Leifeld, J. 2006. Application of diffuse reflectance FT-IR spectroscopy and partial least-squares regression to predict NMR properties of soil organic matter. *European Journal of Soil Science*, **57** (6), 846–857.

Ludwig, B., Nitschke, R., Terhoeven-Urselmans, T., Michel, K. & Flessa, H. 2008. Use of mid-infrared spectroscopy in the diff use-reflectance mode for the prediction of the composition of organic matter in soil and litter. *Journal of Plant Nutrition and Soil Science-Zeitschrift Fur Pflanzenernahrung Und Bodenkunde,* **171** (3), 384–391.

Mathes, N., Xu, Z., Berners-Price, S., Perera, M. & Saffigna, P. 2002. Hydrofluoric acid pre-treatment for improving 13c cpmas nmr spectral qual-ity of forest soils in south-east queensland, australia. *Australian Journal of Soil Research,* **40,** 655–674.

Miller, C. E. 2001. Chemical principles of near-infrared technology. In: Williams, P., Norris, K. (Eds.), *Near-Infrared Technology in the Agri-cultural and Food Industries.* Springer-Verlag New York, Inc.

Mullen, K., Ardia, D., Gil, D. L., Windover, D. & Cline, J. 2011. Deoptim: An r package for global optimization by differential evolution. *Journal of Statistical Software*, **40** (6), 1–26.

Oades, J. M., Vassallo, A. M., Waters, A. G. & Wilson, M. A. 1987. Characterization of organic matter in particle size and density fractions from a red-brown earth by solid state 13c nmr. *Soil Research*, **25,** 71–82.

Paré, M. C. & Bedard-Haughn, A. 2013. Soil organic matter quality influences mineralization and ghg emissions in cryosols: a field-based study of sub-to high arctic. *Global Change Biology*, **19** (4), 1126–1140.

Price, K., Storn, R. M. & Lampinen, J. A. 2006. *Differential evolution: a practical approach to global optimization*. Springer Science & Business Media.

R Core Team, 2020. R: A Language and Environment for Statistical Computing. R Foundation for Statistical Computing, Vienna, Austria. URL https://www.R-project.org/

Sanderman, J., Farrell, M., Macreadie, P., Hayes, M., McGowan, J. & Baldock, J. 2004. Is demineralization with dilute hydrofluoric acid a viable method for isolating mineral stabilized soil organic matter? *Geoderma*, **304**, 4–11.

Savitzky, A. & Golay, M. 1964. Smoothing and differentiation of data by simplified least squares procedures. *Analytical chemistry*, **36,** 1627–1639.

Schmidt, M. W. I., Torn, M. S., Abiven, S., Dittmar, T., Guggenberger, G., Janssens, I. A., Kleber, M., K¨ogel-Knabner, I., Lehmann, J., Manning, D. A. C., Nannipieri, P., Rasse, D. P., Weiner, S. & Trumbore, S. E. 2011. Persistence of soil organic matter as an ecosystem property. *Nature*, **478,** 49–56.

Soriano-Disla, J. M., Janik, L. J., Viscarra Rossel, R. A., Macdonald, L. M. & McLaughlin, M. J. 2014. The Performance of Visible, Near-, and Mid-Infrared Reflectance Spectroscopy for Prediction of Soil Physical, Chemi-cal, and Biological Properties. *Applied Spectroscopy Reviews,* **49** (2), 139–186.

Stenberg, B., Viscarra Rossel, R. A., Mouazen, A. M. & Wetterlind, J. 2010. Visible and near infrared spectroscopy in soil science. *Advances in Agronomy*, **107**, 163–215.

Terhoeven-Urselmans, T., Michel, K., Helfrich, M., Flessa, H. & Ludwig, B. 2006. Near-infrared spectroscopy can predict the composition of organic matter in soil and litter. *Journal of Plant Nutrition and Soil Science-Zeitschrift Fur Pflanzenernahrung Und Bodenkunde* **169** (2), 168–174.

Tinti, A., Tugnoli, V., Bonora, S. & Francioso, O. 2015. Recent applications of vibrational mid-infrared (IR) spectroscopy for studying soil components: a review. *Journal of Central European Agriculture*, **16** (1), 1–22.

Vapnik, V. N. 1995. *The nature of statistical learning theory*. Springer-Verlag New York, Inc.

Viscarra Rossel, R. & McBratney, A. 1998. Soil chemical analytical accuracy and costs: Implications from precision agriculture. *Australian Journal of Experimental Agriculture*, **38** (7), 765–775.

Viscarra Rossel, R. A. & Behrens, T. 2010. Using data mining to model and interpret soil diffuse reflectance spectra. *Geoderma,* **158** (1–2), 46–54.

Viscarra Rossel, R. A. & Hicks, W. S. 2015. Soil organic carbon and its fractions estimated by visible-near infrared transfer functions. *European Journal of Soil Science*, **66,** 438–450.

Viscarra Rossel, R. A., Lee, J., Behrens, T., Luo, Z., Baldock, J. & Richards, A. 2019. Continental-scale soil carbon composition and vulnerability modulated by regional environmental controls. *Nature Geoscience*, **12** (7), 547–552.

Weng, Z., Lehmann, J., Zwieten, L. V., Joseph, S., Archanjo, B. S., Cowie, B., Thomsen, L., Tobin, M. J., Vongsvivut, J., Klein, A., Doolette, C. L., Hou, H., Mueller, C. W., Lombi, E. & Kopittke, P. M. 2021. Probing the nature of soil organic matter. *Critical Reviews in Environmental Science and Technology*

FIGURE CAPTIONS

Figure 1 Location of the 99 soil samples a), and soil texture b) and soil organic carbon content (SOC) c) in the samples.

Figure 2 Summary of the NMR spectra form the 99 soil samples with a) showing the median and 16^{th} and 84^{th} percentile NMR spectrum with the different functional C groups and subgroups indicated, and b) showing NMR spectra representing three common types of NMR spectra in the data set, i.e. those with a high, low and intermediate ratio of alkyl C to O/N-alkyl C.

Figure 3 2D correlation plots between a) vis–NIR and NMR, and b) mid-IR and NMR. Blue colour indicates negative correlations and red indicates positive correlations. Black spectra shows the average original absorbance IR spectra and relative intensity NMR spectra, and red the average base lined spectra used in the correlations.

Figure 4 Cross validated predictions versus measured SOC content (a, d), relative contribution of alkyl C CH_2-C groups (alkyl C subgroup 2) (b, e), and alkyl C:O/N-alkyl C ratio derived from relativ contribution (c, f) using machine learning models based on mid-IR (a-c) and vis–NIR (d-f) spectra. Red dotted lines are polynomial fits that show deviations from the linear fits. The predictions are average of the five repeated cross validations.

Figure 5 The importance of different wavelength in the machine learning models for total C content, relative contribution of the different NMR-derived functional carbon groups and subgroups, and the ratio between alkyl C and O/N-alkyl C derived from relative contribution using the a) vis–NIR and b) mid-IR wavelength range.

TABLES

Table 1 Cross-validated prediction results for the vis–NIR calibration models, and the final hyperparameters used (sigma, C), for SOC (%), relative contribution of the different ^{13}C NMR derived C groups (%), and the Alkyl C:O/N-alkyl C ratio derived from relative contribution. The predictions are average results of five times repeated 10-fold cross-validation.

	R^2	CCC	RMSE	ME	sigma	C
SOC	0.62	0.75	1.3	-0.207	0.00052	8.735
Alkyl C	0.83	0.91	3.0	0.090	0.00112	9.085
subgroup 1	0.56	0.74	1.6	0.087	0.00074	8.746
subgroup 2	0.84	0.91	2.0	-0.006	0.00110	8.199
O/N-alkyl C	0.34	0.56	2.6	-0.037	0.00187	8.479
subgroup 1	0.10	0.28	0.6	-0.014	0.00254	2.321
subgroup 2	0.26	0.44	1.7	0.027	0.00581	6.312
subgroup 3	0.70	0.82	0.6	0.026	0.00096	7.075
Aryl C	0.77	0.87	1.8	-0.144	0.00109	9.105
subgroup 1	0.73	0.84	1.2	-0.116	0.00111	7.355
subgroup 2	0.71	0.83	0.9	-0.002	0.00184	5.099
Carboxyl C	0.64	0.78	1.4	0.034	0.00123	8.531
subgroup 1	0.64	0.79	0.8	0.012	0.00116	7.466
subgroup 2	0.46	0.65	0.9	0.008	0.00552	3.535
Alkyl C: O/N-alkyl C	0.81	0.89	0.1	-0.007	0.00186	7.573

Table 2 Cross-validated prediction results for the mid-IR calibration models, and the final hyperparameters used, for SOC (%), relative contribution of the different ^{13}C NMR derived C groups (%), and the Alkyl C:O/N-alkyl C ratio derived from relative contribution. The predictions are average results of five times repeated 10-fold cross-validation.

	R^2	CCC	RMSE	ME	sigma	C
SOC	0.86	0.92	0.8	-0.02	0.00053	5.841
Alkyl C	0.85	0.92	2.7	0.35	0.00048	9.024
subgroup 1	0.56	0.73	1.5	0.088	0.00027	9.137
subgroup 2	0.92	0.96	1.5	-0.017	0.00031	8.961
O/N-alkyl C	0.38	0.60	2.2	-0.003	0.00035	8.577
subgroup 1	0.32	0.54	0.5	0.017	0.00056	6.117
subgroup 2	0.20	0.42	1.7	-0.001	0.00075	7.366
subgroup 3	0.73	0.85	0.6	-0.054	0.00034	9.372
Aryl C	0.72	0.85	2.1	-0.098	0.00082	8.768
subgroup 1	0.71	0.83	1.3	-0.133	0.00039	5.835
subgroup 2	0.81	0.90	0.7	0.049	0.00062	9.955
Carboxyl C	0.54	0.73	1.5	0.006	0.00048	8.188
subgroup 1	0.63	0.77	0.7	-0.026	0.00025	9.126
subgroup 2	0.35	0.56	0.9	-0.10	0.00056	5.320
Alkyl C: O/N-alkyl C	0.84	0.91	0.1	0.00	0.00051	9.138

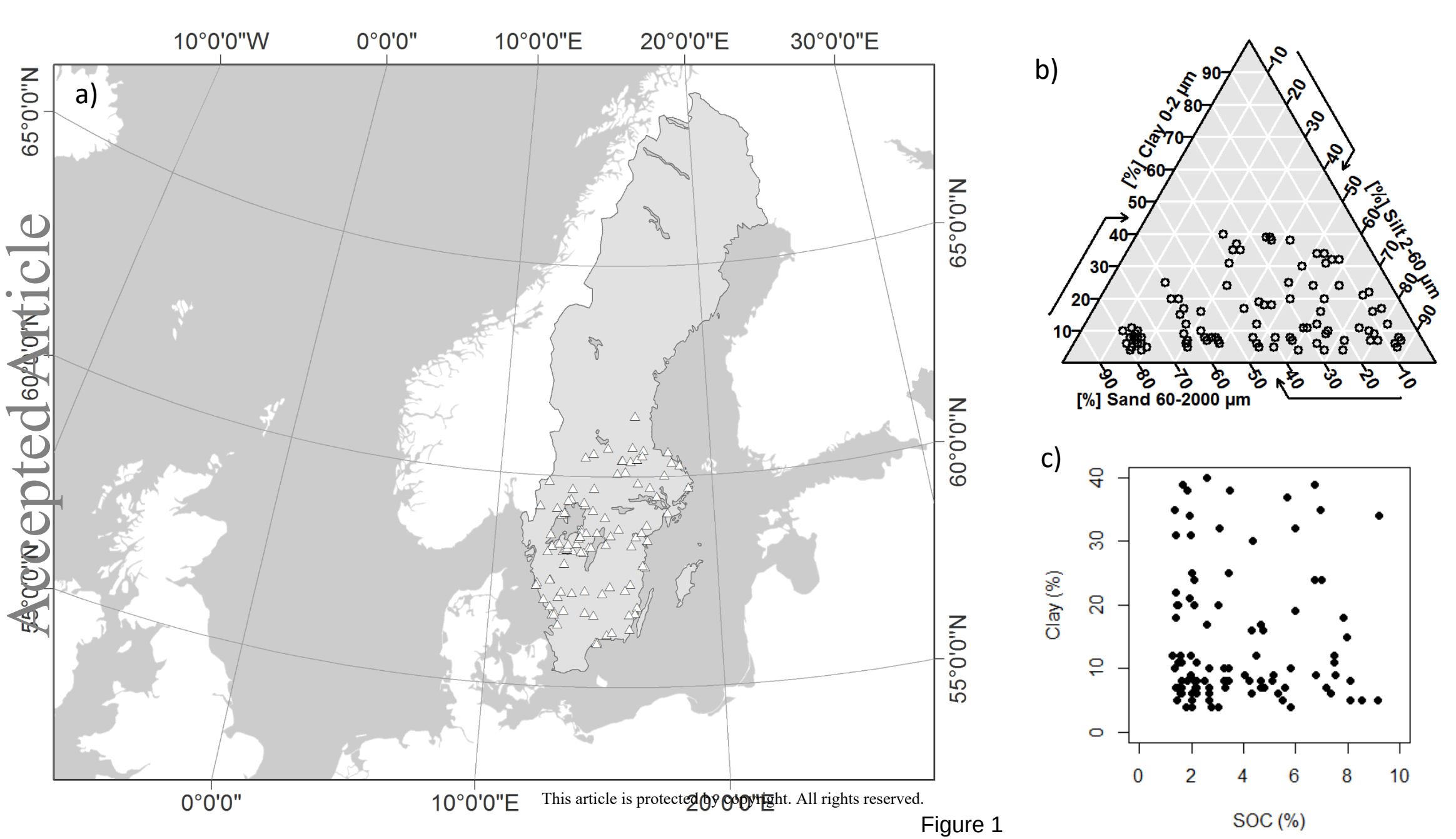

Figure 1

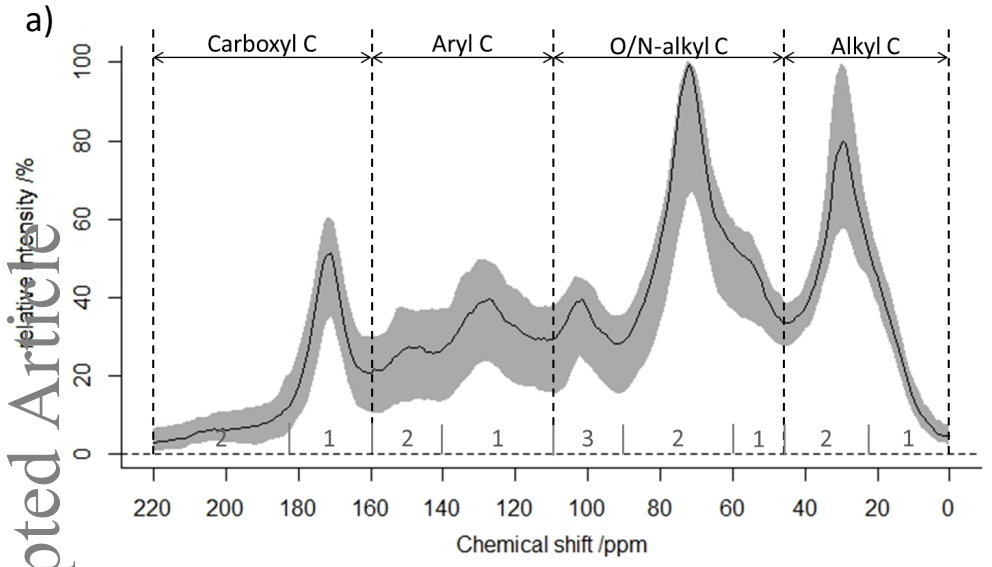

Alkyl C	subgroup 1	terminal CH_3-groups
	subgroup 2	CH_2 groups
O/N-alkyl C	subgroup 1	methoxyl C, C in amino groups
	subgroup 2	carbohydrate C, C-OH groups
	subgroup 3	acetal C, ketal C
Aryl C	subgroup 1	protonated and non-substituted aromatic C
	subgroup 2	N- or O-substituted aromatic C
Carboxyl C	subgroup 1	carboxylic C
	subgroup 2	carbonylic C

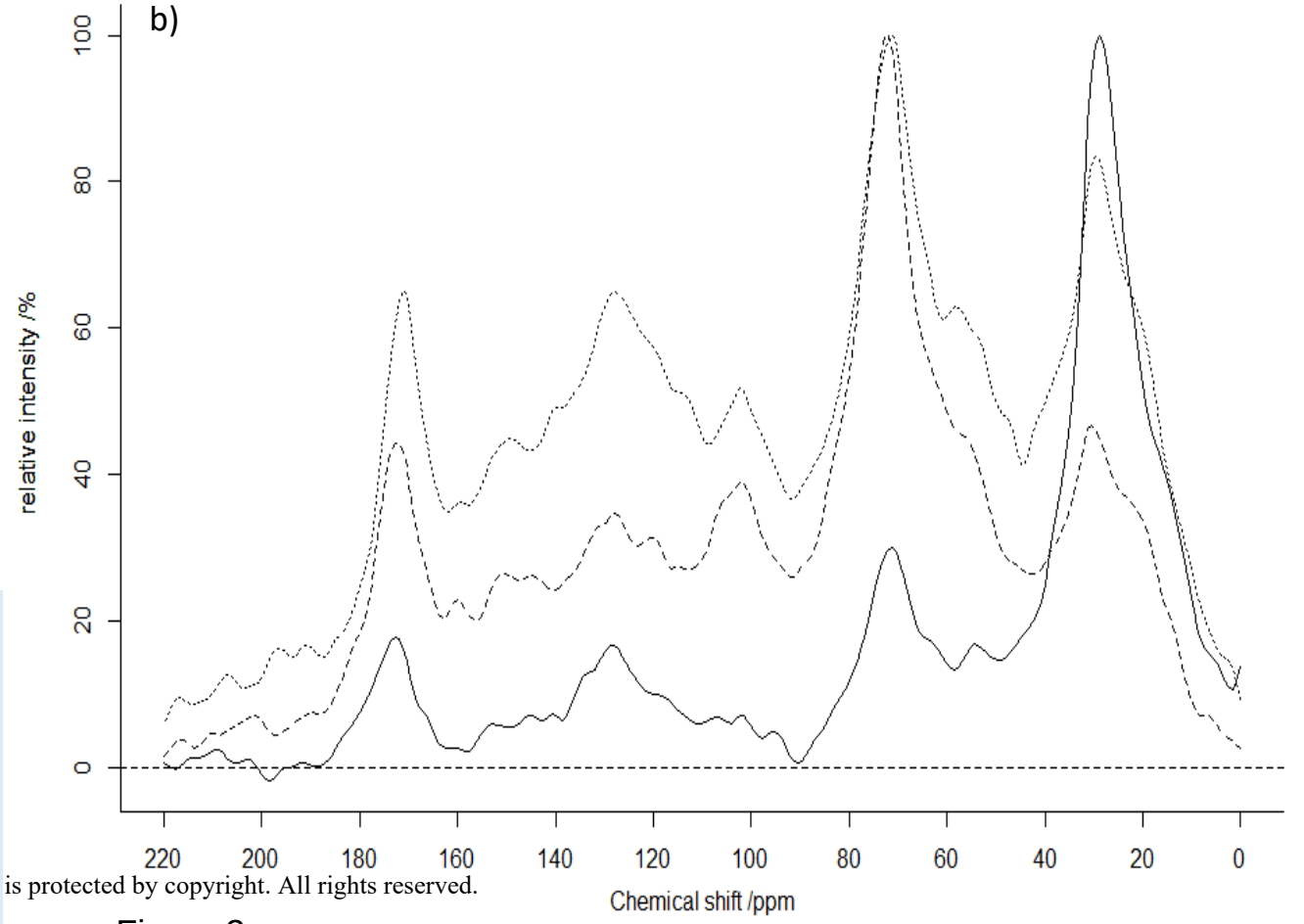

Figure 2

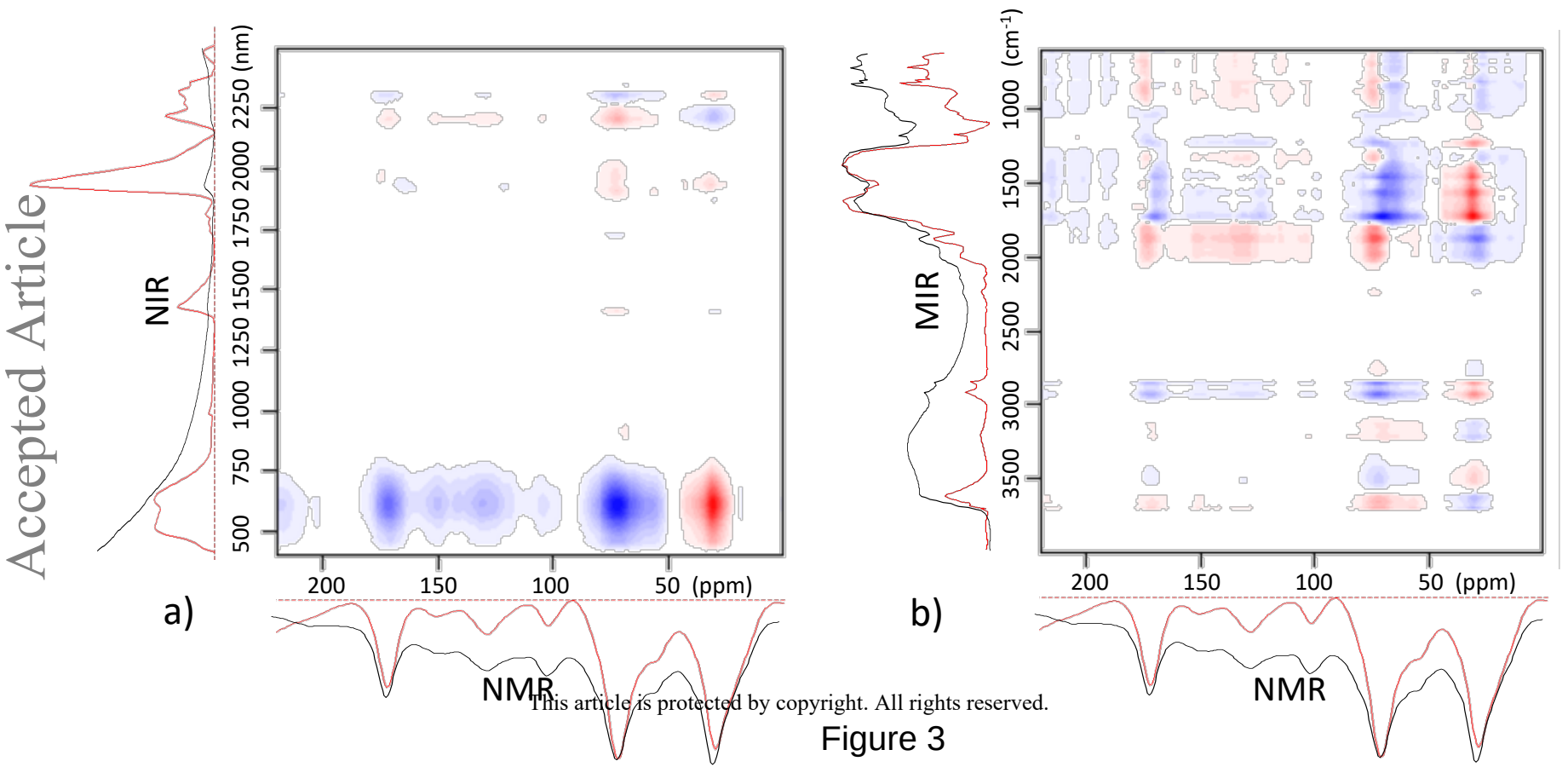

Figure 3

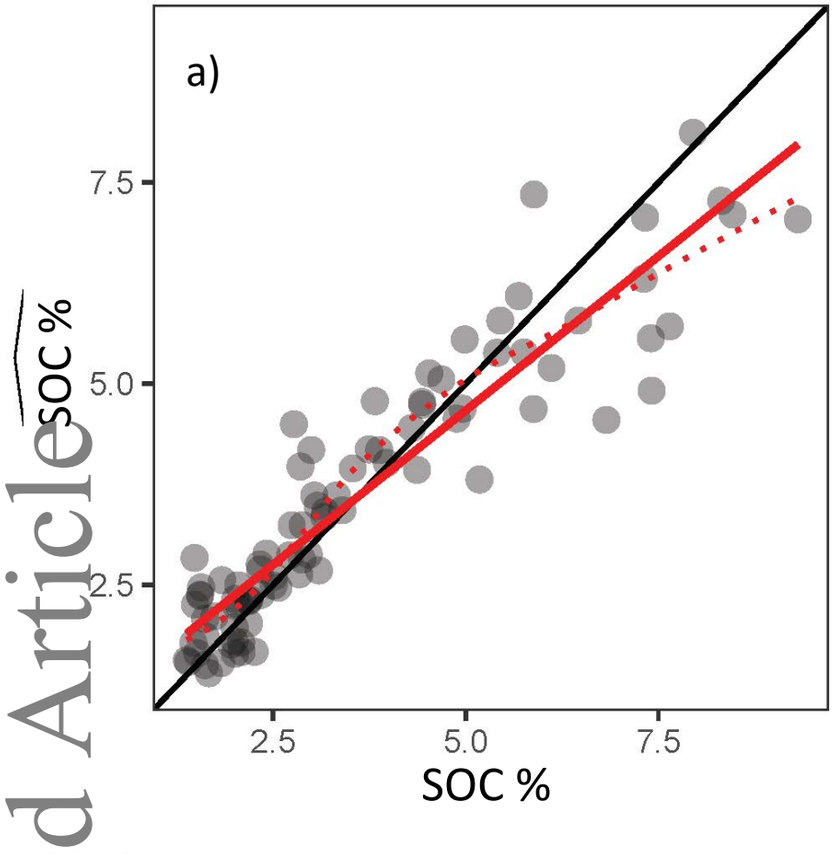

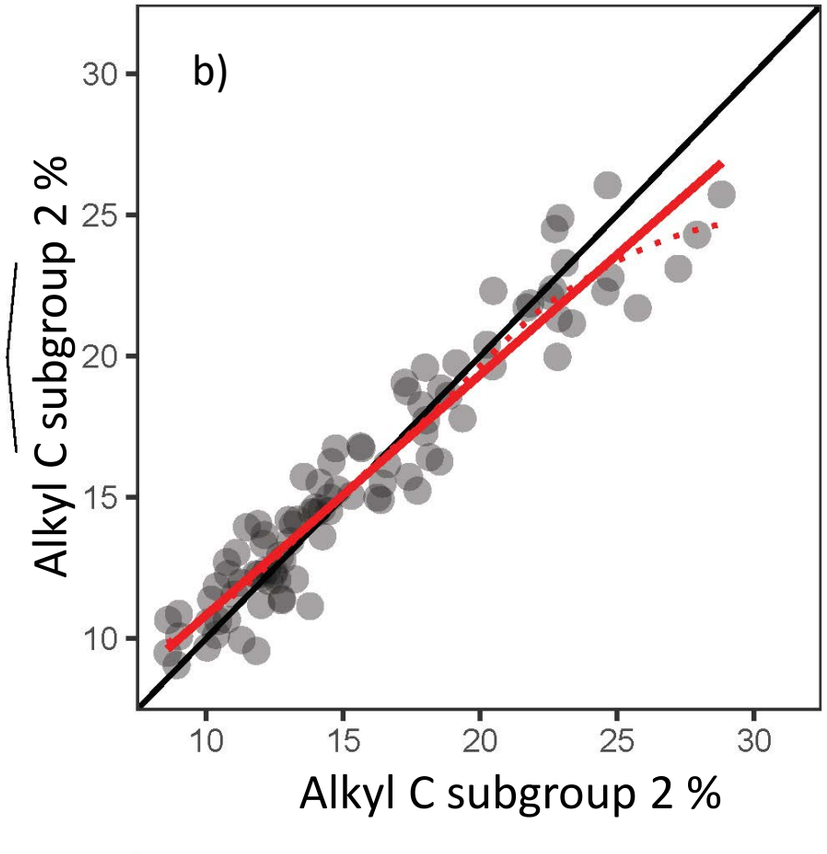

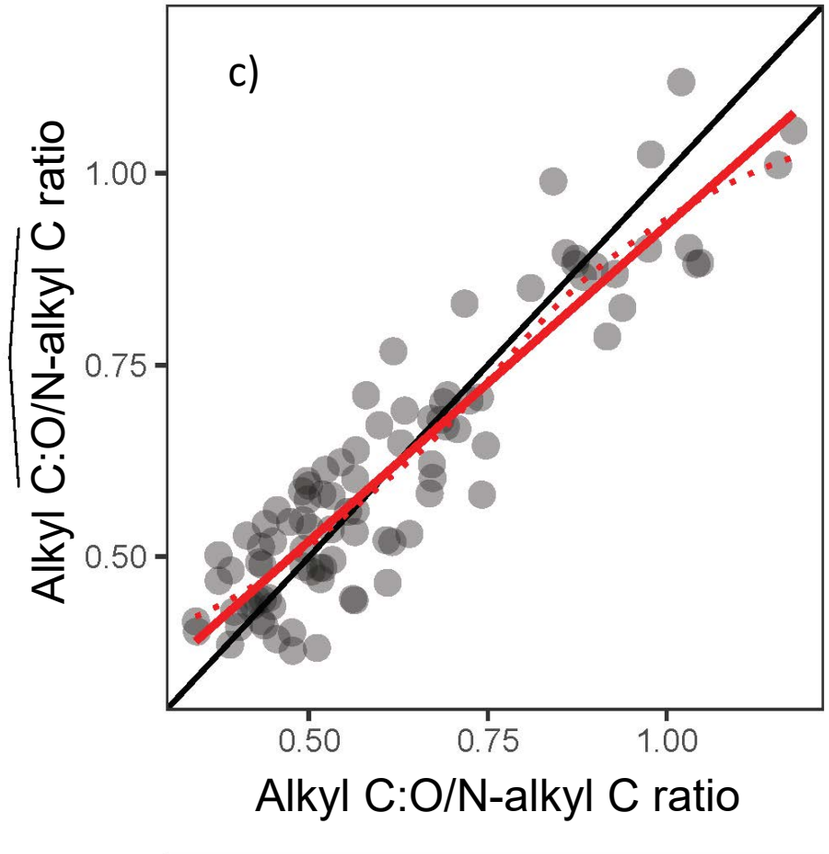

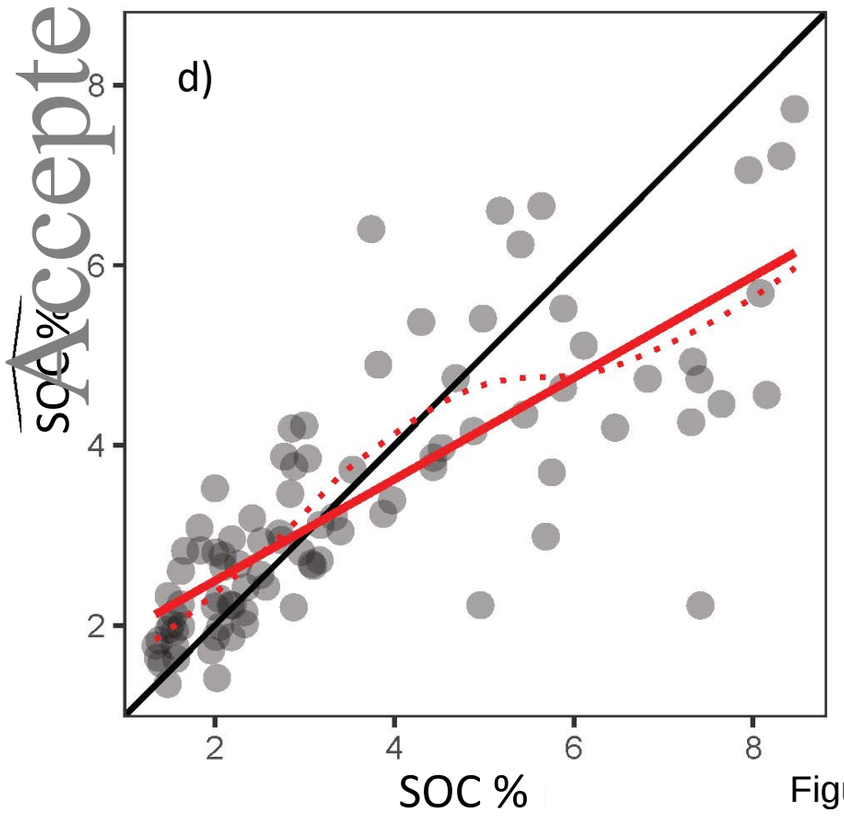

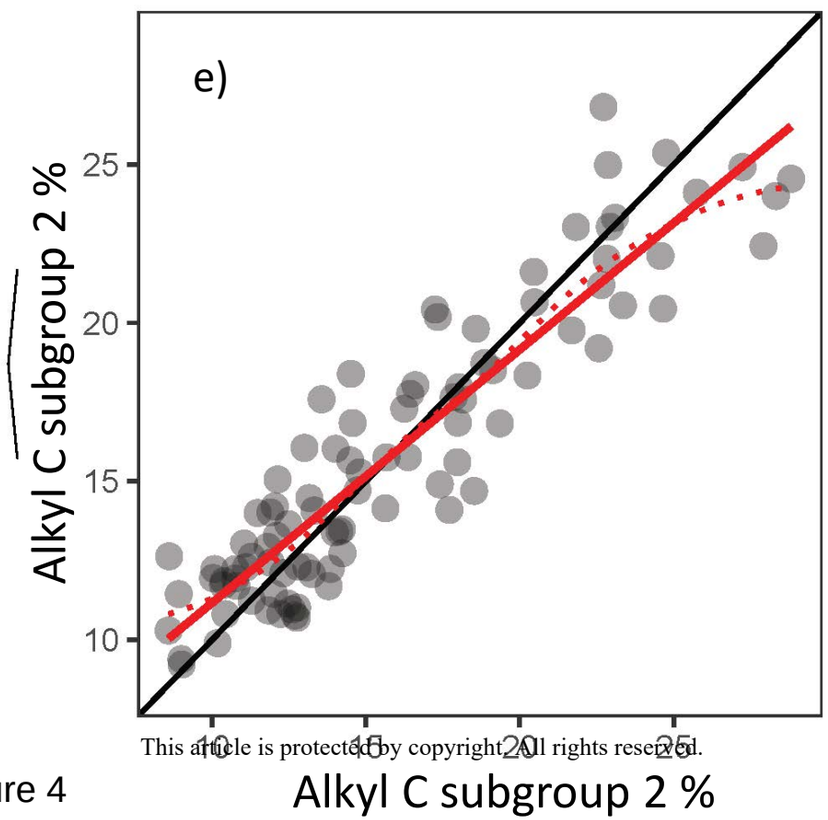

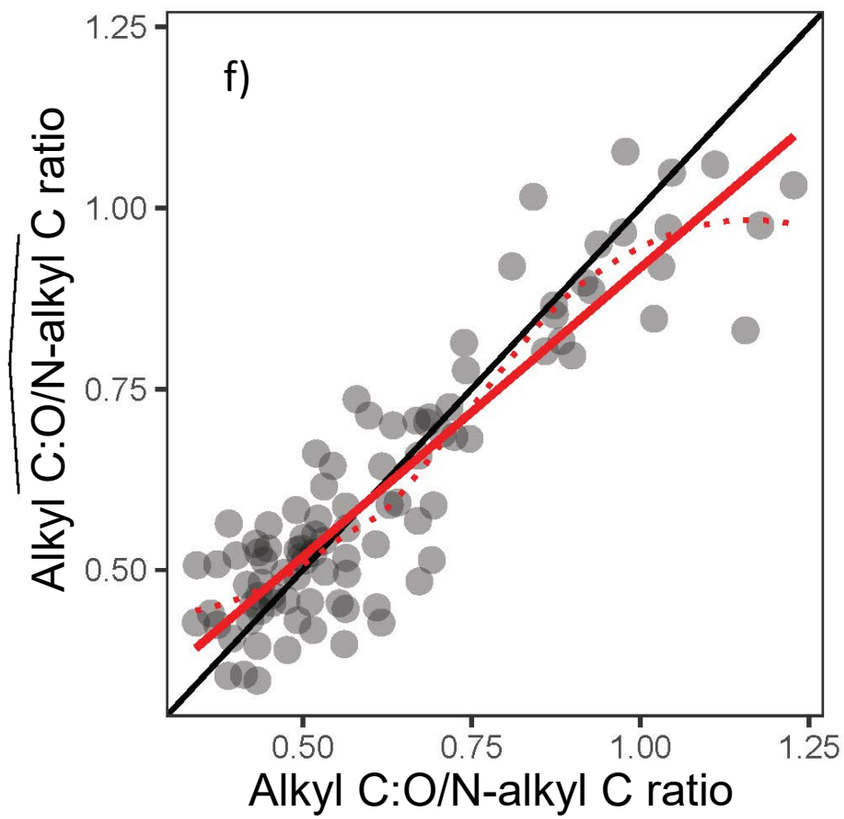

Figure 4

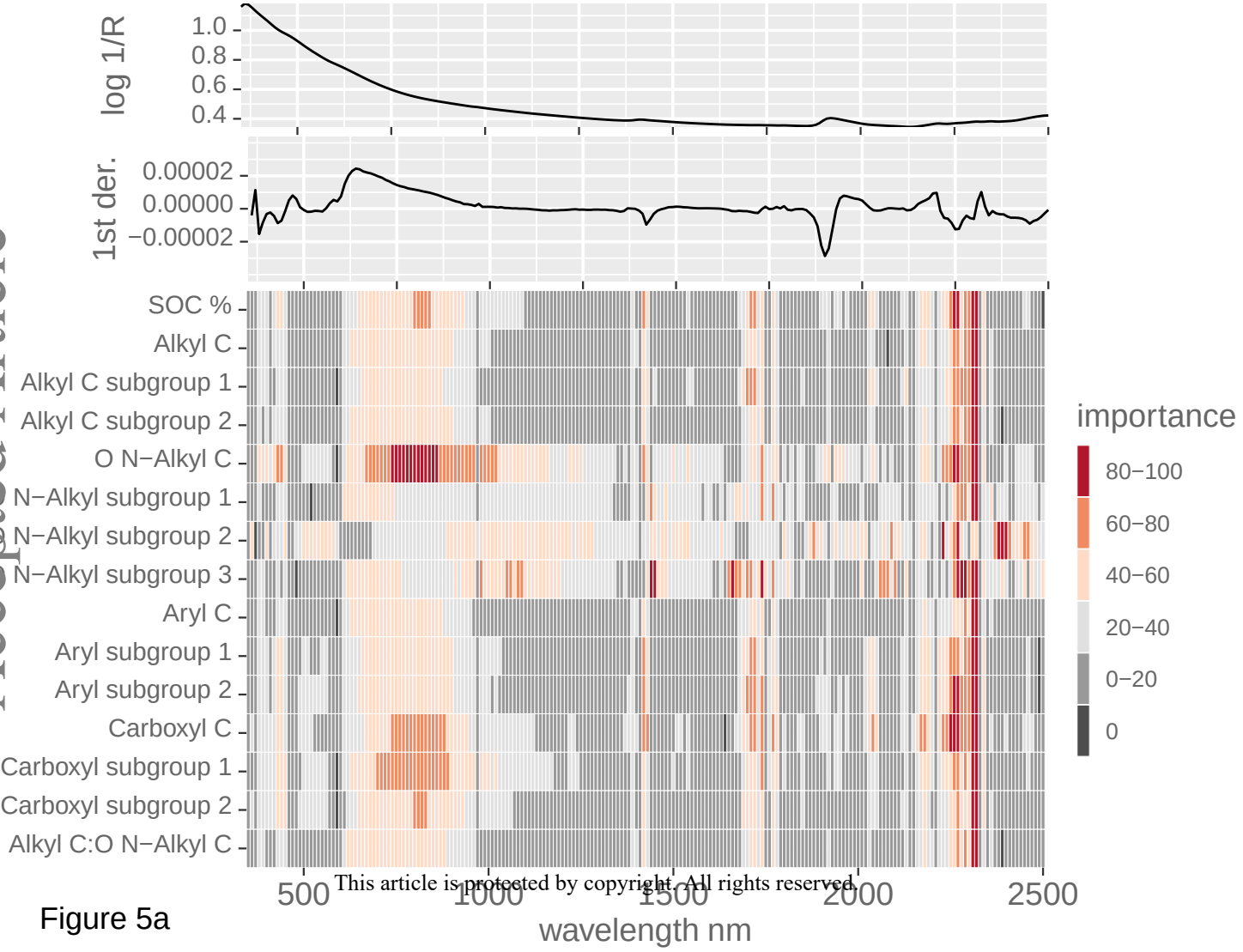

Figure 5a

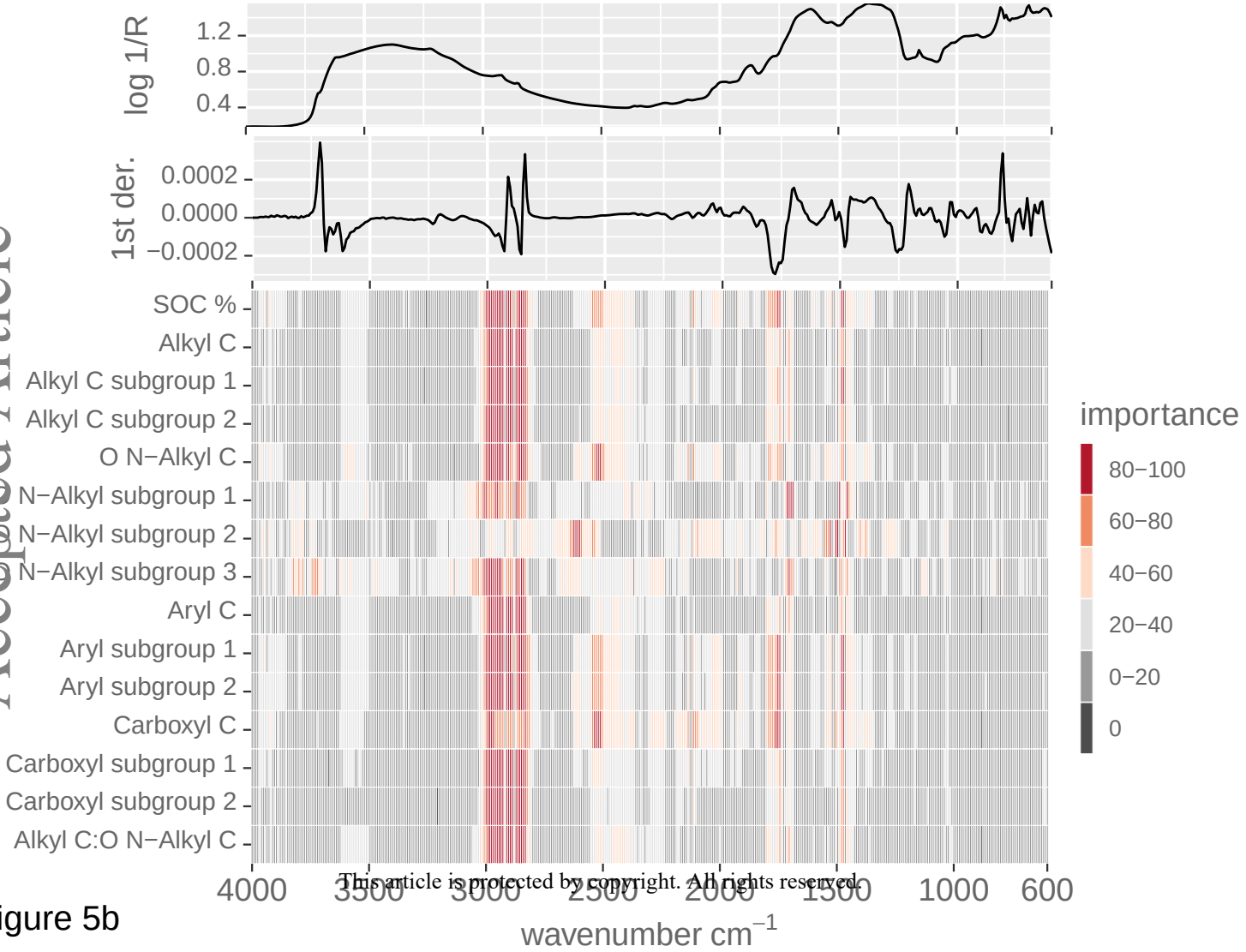

Figure 5b